

# Second-order nonlinear mixing in planar photonic crystal microcavities

Murray W. McCutcheon, Georg W. Rieger, and Jeff F. Young

Department of Physics and Astronomy, University of British Columbia, Vancouver, Canada, V6T 1Z1

Dan Dalacu, Simon Frédéric\*, Philip J. Poole, and Robin L. Williams\*

Institute for Microstructural Sciences, National Research Council, Ottawa, Canada, K1A 0R6

\*Also at: Physics Department, University of Ottawa, Ottawa, Canada, K1N 6N5

[murray@phas.ubc.ca](mailto:murray@phas.ubc.ca)

**Abstract:** Second-harmonic and sum-frequency mixing phenomena associated with 3D-localized photonic modes are studied in InP-based planar photonic crystal microcavities excited by short-pulse radiation near 1550 nm. Three-missing-hole microcavities that support two closely-spaced modes exhibit rich second-order scattering spectra that reflect intra- and inter-mode mixing via the bulk InP  $\chi^{(2)}$  during ring-down after excitation by the broadband, resonant pulse. Simultaneous excitation with a non-resonant source results in tunable second-order radiation from the microcavity.

© 2018 Optical Society of America

**OCIS codes:** (230.5750) Resonators; (190.2620) Frequency conversion; (190.4390) Nonlinear optics, integrated optics

## References and links

1. K. Sakoda and K. Ohtaka, "Sum-frequency generation in a two-dimensional photonic lattice," *Phys. Rev. B* **54**, 5742–5749 (1996).
2. M. Soljačić and J. D. Joannopoulos, "Enhancement of nonlinear effects using photonic crystals," *Nature Mat.* **3**, 211–219 (2004).
3. A. R. Cowan and J. F. Young, "Nonlinear optics in high refractive index contrast periodic structures," *Semicond. Sci. Technol.* **20**, R41–R56 (2005).
4. P. E. Barclay, K. Srinivasan, and O. Painter, "Nonlinear response of silicon photonic crystal microresonators excited via an integrated waveguide and fiber taper," *Opt. Express* **13**, 801–820 (2005), <http://www.opticsexpress.org/abstract.cfm?URI=OE-13-3-801>.
5. D. K. Armani, T. J. Kippenberg, S. M. Spillane, and K. J. Vahala, "Ultra-high- $Q$  toroid microcavity on a chip," *Nature* **421**, 925–928 (2003).
6. T. J. Kippenberg, S. M. Spillane, and K. J. Vahala, "Kerr-Nonlinearity optical parametric oscillation in an ultrahigh- $Q$  toroid microcavity," *Phys. Rev. Lett.* **93**, 083904 (2004).
7. T. J. Johnson, M. Borselli, and O. Painter, "Self-induced optical modulation of the transmission through a high- $Q$  silicon microdisk resonator," *Opt. Express* **14**, 817–831 (2006). <http://www.opticsexpress.org/abstract.cfm?URI=OE-14-2-817>.
8. K. J. Vahala, "Optical microcavities," *Nature* **424**, 839–846 (2003).
9. H. J. Kimble, "Strong interactions of single atoms and photons in cavity QED," *Phys. Scr. T76*, 127–137 (1998).
10. J. Trull, R. Vilaseca, J. Martorell, and R. Corbalán, "Second-harmonic generation in local modes of a truncated periodic structure," *Opt. Lett.* **20**, 1746–1748 (1995).
11. T. V. Dolgova, A. I. Maidykovski, M. G. Martemyanov, A. A. Fedyanin, O. A. Aktsipetrov, G. Marowsky, V. A. Yakovlev, and G. Mattei, "Giant microcavity enhancement of second-harmonic generation in all-silicon photonic crystals," *Appl. Phys. Lett.* **81**, 2725–2727 (2002).
12. A. R. Cowan and J. F. Young, "Mode matching for second-harmonic generation in photonic crystal waveguides," *Phys. Rev. B* **65**, 085106 (2002).
13. J. P. Mondia, H. M. van Driel, W. Jiang, A. R. Cowan, and J. F. Young, "Enhanced second-harmonic generation from planar photonic crystals," *Opt. Lett.* **28**, 2500–2502 (2003).

14. O. Painter and K. Srinivasan, "Localized defect states in two-dimensional photonic crystal slab waveguides: a simple model based upon symmetry analysis," *Phys. Rev. B* **68**, 035110 (2003).
15. M. W. McCutcheon, G. W. Rieger, I. W. Cheung, J. F. Young, D. Dalacu, S. Frédérick, P. J. Poole, G. C. Aers, and R. L. Williams, "Resonant scattering and second-harmonic spectroscopy of planar photonic crystal microcavities," *Appl. Phys. Lett.* **87**, 221110 (2005).
16. K. J. Resch and A. M. Steinberg, "Extracting joint weak values with local, single-particle measurements," *Phys. Rev. Lett.* **92**, 130402 (2004).
17. G. J. Pryde, J. L. O'Brien, A. G. White, T. C. Ralph, and H. M. Wiseman, "Measurement of quantum weak values of photon polarization," *Phys. Rev. Lett.* **94**, 220405 (2005).

## 1. Introduction

Microfabricated structures in semiconductor thin films offer the opportunity to tightly confine light in nonlinear, transparent media [1, 2, 3, 4]. Various micro-disk and micro-toroid structures have been fabricated in semiconductor membranes to act as ultrasmall optical cavities that support discrete microcavity modes with very high quality (Q) factors in excess of  $10^8$  [5]. These exhibit optical bistability and other nonlinear responses at exceedingly low optical powers when coupled efficiently to single mode waveguides [6, 7]. Engineered defect states within planar photonic crystals (PPCs) offer an alternative to micro-disk/toroid-based cavities: currently they have not been produced with as high Q values, but their mode volumes ( $V_m$ ) are smaller, so that the ratio of their Q values to their mode volumes are comparable, or even larger.  $Q/V$  or  $Q/\sqrt{V_m}$  are figures of merit for cavity-based quantum electrodynamic (cavity QED) phenomena, which provides yet another motivation for developing ultrasmall nonlinear structures [8, 9]. Enhanced second-harmonic generation (SHG) has been observed in 1D photonic crystal microcavities with dielectric [10] and mesoporous silicon Bragg mirrors [11]. Previous work studying SHG in PPC slabs showed that when one or both of the fundamental and second-harmonic beams are mode-matched to leaky modes of the structure, there is a significant resonant enhancement of the radiated second harmonic [12, 13]. This effect was shown to be due to the local field enhancements associated with the incoming and outgoing resonances.

In this letter, we report on the second-order response of the 3D-localized states of a PPC microcavity in a sub-wavelength thick semiconductor slab that is locally excited by a diffraction-limited beam *incident perpendicular to the slab*. The mode energies, and hence the second-order radiation energies, can be controlled by tailoring the photonic crystal defect lattice that defines the microcavity [14].

## 2. Experiment

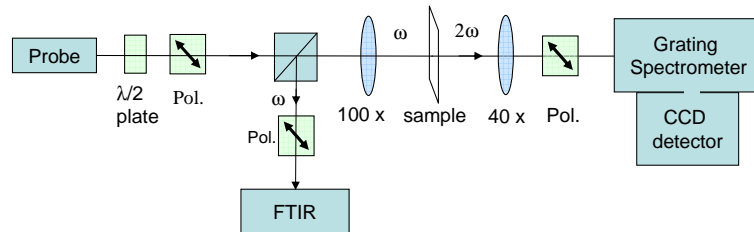


Fig. 1. Schematic of the experimental set-up. The linear spectra are obtained from the reflected resonantly scattered radiation, and detected in the cross-polarization using a Fourier transform infrared (FTIR) spectrometer. The second-order radiation is detected (simultaneously) in a transmission geometry.

The slab which hosts the PPC microcavity is a 230nm thick [001]-oriented InP free-standing membrane mounted on a glass substrate. It is excited by a train of pulses from a 80 MHz

optical parametric oscillator (OPO) (Spectra Physics) pumped at 810 nm and focussed through a 100x microscope objective lens [15]. As shown in the optical set-up in Figure 1, the resonantly scattered light is collected in reflection, and detected in the cross-polarization with respect to the incident beam using a Bomem Fourier transform infrared spectrometer. The second-order radiation is collected in transmission using a 40 $\times$  (NA=0.65) microscope objective, and detected using a grating spectrometer and a liquid-nitrogen cooled CCD detector.

### 3. Results

The linear resonant scattering spectrum from a three-missing-hole (3h) cavity which supports a single mode is shown in Figure 2(a). The non-resonant background, which has the shape of the excitation spectrum, is radiated by polarization driven by the OPO source while it directly interacts with the thin slab. The resonant feature is due to lingering polarization induced by the electric field scattered into the resonant mode of the cavity as it “rings down” [15]. When the spectrometer is set to twice the frequency, the resulting SHG spectrum (b) closely mimics the linear spectrum. The broad peak is also observed when the untextured InP slab is irradiated by the same beam. This *non-resonant* second-order scattering corresponds to the second-order interaction between the laser pulse and the InP slab. The sharp feature at exactly twice the mode frequency corresponds to the second-order polarization induced by the mode, as it rings down, via the  $\chi^{(2)}$  of the InP slab.

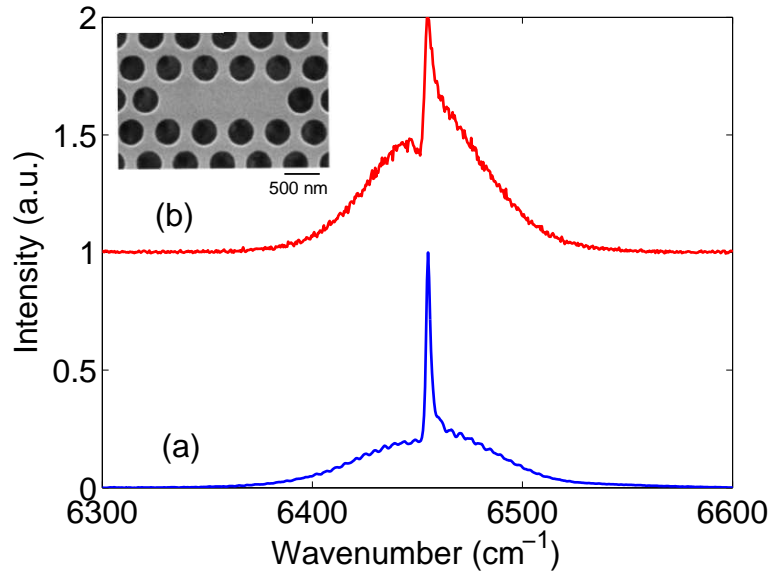


Fig. 2. (a) Linear and (b) second-order (plotted at half the energy) spectra from the high Q mode of an InP 3-h microcavity. An SEM image of the microcavity is shown in the inset.

When a microcavity supports two modes, the second-order spectra are more complex. Spectra from a 3h-cavity with two closely-spaced modes are shown in Figure 3. The linear scattering spectrum (blue) shows two resonant features at  $6300\text{ cm}^{-1}$  and  $6330\text{ cm}^{-1}$ , superimposed on a non-resonant background from the scattered laser spectrum used to excite the sample. In the second-order spectrum (red), which is plotted at half the energy, the lowest and highest energy peaks are at exactly twice the frequencies of the microcavity modes evident in the linear spectra, and the central sharp feature, at  $6315\text{ cm}^{-1}$ , is at precisely their sum frequency. These resonant features in the nonlinear scattering spectrum therefore correspond to second-order intra- and

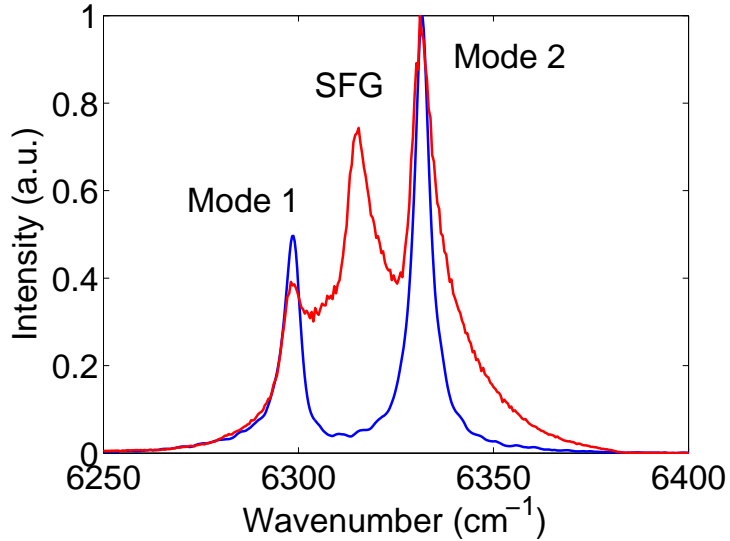


Fig. 3. Linear (blue) and nonlinear (red) resonant scattering from a two-mode 3-h microcavity. The nonlinear spectrum is plotted at half the energy, and shows an additional feature due to sum-frequency generation (SFG) of the modes.

inter-mode interactions of the fields, which are resonantly scattered into the microcavity modes from the femtosecond (fs) pulses, as the energy in the cavity decays due to out-of-plane (linear) scattering. The sum-frequency generation (SFG) associated with the inter-mode interaction provides a weak probe of the mode occupation(s). This signal is only non-zero when two modes are excited in the microcavity, and it may therefore be applicable in weak quantum measurement schemes [16, 17].

The electric fields trapped in the microcavity modes can also be used to generate second-order radiation at different frequencies via sum-frequency mixing with a separate field incident on the structure. This is illustrated in Figure 4, where a series of four second-order spectra from the same microcavity as in Fig. 3 are shown when simultaneously excited by short, resonant pulses (as in Fig. 3), and longer, picosecond (ps) pulses tuned far off resonance with the microcavity modes. This two-colour source is readily available from the unfiltered “signal” beam output of the OPO when it is tuned near the degeneracy point (where both signal and idler frequencies are close to half the pump frequency). An example of this unfiltered spectrum when the signal is tuned to  $6320\text{ cm}^{-1}$  is shown as the solid red curve (b) in Figure 4. The short OPO signal pulses are accompanied by relatively long (a few ps) OPO idler pulses at a centre frequency roughly equal to the difference between the pump and signal frequencies. The centre frequency of these ps pulses converges with the signal beam frequency at half the pump frequency as the OPO is tuned.

The second-order spectra show three principal groups of features that are marked by lines A, B, and C to guide the eye. Feature A and the broad background in group C (the fit of which is plotted separately as a dashed red line), are the second-harmonics of the ps and fs features, respectively, in the excitation spectra. These features, which shift at the same rate as the corresponding features in the excitation spectra, are due to non-resonant second-order scattering, as observed in Fig. 2.

The three sharp features in group C that do not shift, and the two sharp features in group

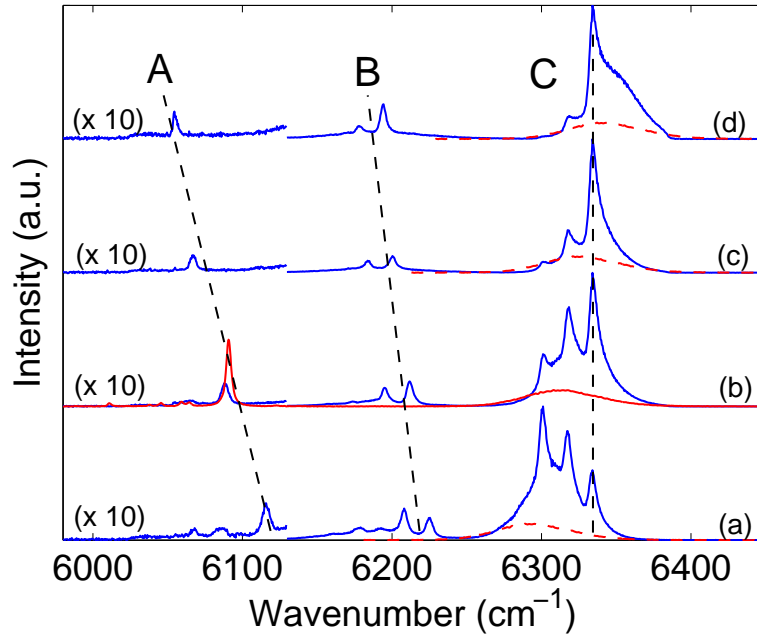


Fig. 4. Spectra obtained from the interaction of a non-resonant, narrow linewidth idler pulse; a broad resonant laser pulse; and a two-mode PPC microcavity. The blue curves (a)-(d) show the second-order response, plotted at half the energy, as the OPO is tuned to higher energy. In each spectrum, the amplitude of the low energy region has been multiplied by 10 for clarity. The solid red curve (b) shows the laser spectrum scattered from an untextured part of the InP slab. The non-resonant second-order laser background is shown schematically by the dashed red curves. The features A, B, and C are discussed in detail in the text.

B that shift at half the rate of the excitation beam(s), are specific to the microcavity modes. They all reflect second-order processes that involve the fields “trapped” in at least one of the modes, as they ring down. The three (fixed) peaks in group C correspond to the mode SHG and SFG features, as in Figure 3. The features in group B are then easily understood to result from the second-order radiation of the two field distributions trapped in the microcavity modes respectively interacting with the ps pulses that are constantly irradiating the cavity during the ring-down. To understand the difference in the shift rate between features A and B, consider a ps pulse at  $\omega_A$  interacting with a microcavity mode at  $\omega_C$ . When the ps pulse is tuned from  $\omega_A$  to  $\omega_A - \Delta\omega$ , the second-order feature A shifts from  $2\omega_A$  to  $2(\omega_A - \Delta\omega)$ , which is a shift of  $-2\Delta\omega$ , whereas feature B shifts from  $\omega_A + \omega_C$  to  $\omega_A - \Delta\omega + \omega_C$ , a shift of just  $-\Delta\omega$ . The processes illustrated here demonstrate that the fields stored in microcavity modes can be used in conjunction with tunable sources to produce second-order radiation in a spectral window of choice.

Experimentally, the polarization of the non-resonant second-order radiation associated with the laser background in spectra such as shown in Fig. 2 is virtually unchanged from spectra obtained from an untextured “bulk” part of the InP slab. This suggests that the bulk InP second-order tensor is sufficient to describe the nonlinear polarization generated in the material by the OPO pulses. However, the relationship between the *electromagnetic field polarizations* of

the excitation source and the second-order fields radiated from the resonant modes is quite different, and more complex, in this microcavity geometry than in more familiar bulk or uniform waveguide structures. The second-order polarizations associated with the resonant modes have complex multipole-like distributions, and scattering from the surrounding lattice of air-holes plays an important role in determining the properties of the far-field radiation that is generated. An analysis of the polarization properties of the second-order radiation will be discussed in a forthcoming publication.

#### **4. Summary**

In summary, we have demonstrated second-order intra- and inter-mode nonlinear mixing of 3D-localized modes in a planar photonic crystal defect microcavity. When the microcavity supports a single mode, the second-order spectrum mimics the linear spectrum, showing both non-resonant and resonant features. When the microcavity supports two modes, an additional feature is revealed in the second-order spectrum, due to the nonlinear mixing of both resonant modes. The energy stored in the microcavity modes can be used in conjunction with a separate, nonresonant beam, to generate tunable sum frequency radiation over a broad range of frequencies.

#### **Acknowledgements**

The authors wish to acknowledge the financial support of the Natural Sciences and Engineering Research Council of Canada, the Canadian Institute for Advanced Research, the Canadian Foundation for Innovation, the Canadian Institute for Photonic Innovations, and the technical assistance of Lumerical Solutions Inc.